

Enhanced spin relaxation time due to electron-electron scattering in semiconductors

W.J.H. Leyland* and G.H. John and R.T. Harley

School of Physics and Astronomy, University of Southampton, Southampton SO17 1BJ, UK.

M.M. Glazov and E.L. Ivchenko

A.F.Ioffe Physico-Technical Institute, Russian Academy of Sciences, 194021 St Petersburg, Russia.

D.A. Ritchie

Cavendish Laboratory, Madingley Road, Cambridge CB4 3HE, UK.

A.J. Shields

Toshiba Research Europe Ltd, Milton Road Science Park, Cambridge CB4 4WE, UK

M. Henini

School of Physics and Astronomy, University of Nottingham, Nottingham NG7 4RD, UK

(Dated: April 29, 2019)

We present a detailed experimental and theoretical analysis of the spin dynamics of two-dimensional electron gases (2DEGs) in a series of n -doped GaAs/AlGaAs quantum wells. Picosecond-resolution polarized pump-probe reflection techniques were applied in order to study in detail the temperature-, concentration- and quantum-well-width- dependencies of the spin relaxation rate of a small photoexcited electron population. A rapid enhancement of the spin life-time with temperature up to a maximum near the Fermi temperature of the 2DEG was demonstrated experimentally. These observations are consistent with the D'yakonov-Perel' spin relaxation mechanism controlled by electron-electron collisions. The experimental results and theoretical predictions for the spin relaxation times are in good quantitative agreement.

I. INTRODUCTION

Expectations for device applications of non-equilibrium spin populations of electrons and/or nuclei in semiconductors will become more realistic when there is complete understanding of the microscopic mechanisms which control spin coherence and relaxation. This applies particularly to quantum well structures as they are likely to be an important part of any such spintronic device. In this paper we report an experimental and theoretical study of electron spin relaxation at temperatures between 5 K and 300 K in a series of GaAs/AlGaAs quantum wells containing high mobility two-dimensional electron gases (2DEGs). We have previously published detailed accounts of our theoretical approach^{1,2,3} and preliminary accounts of the experiments on one of the samples⁴. By fully characterizing the electron mobility and concentration and making use of results from an experimental study of low temperature spin dynamics in the same samples, to be published separately⁵, we are able here to give a complete quantitative theoretical description of the spin dynamics in all the samples.

Three mechanisms are known for spin relaxation of electrons in zinc-blende semiconductors^{6,7}. Two usually make minor contributions; these are spin-flips associated with electron scattering due to spin-orbit interaction, the Elliott-Yafet (EY) mechanism^{8,9} and spin-flips induced by exchange interaction with holes, the Bir-Aronov-Pikus (BAP) mechanism¹⁰. The third, the D'yakonov-Perel' (DP) mechanism^{11,12} is the most important particularly

in n -type samples. In the DP mechanism the driving force for spin reorientation is the intrinsic tendency of electron spins to precess in the effective magnetic field which they experience as a result of spin-orbit interaction. This is quantified as the spin-splitting of the conduction band. The corresponding precession vector Ω_k varies in magnitude and direction according to the electron wavevector \mathbf{k} . Under normal conditions in a 2DEG a collision-dominated regime holds in which the electron spin precession is frequently interrupted by scattering causing spin reorientation to proceed as a succession of randomly directed small fractional rotations. Approach to equilibrium is exponential with spin relaxation rate along a particular (main) axis of the structure, i , given by^{7,11}

$$\tau_{s,i}^{-1} = \langle \Omega_{\perp}^2 \rangle \tau_p^* \quad (\langle |\Omega_{\perp}| \rangle \tau_p^* \ll 1), \quad (1)$$

where $\langle \Omega_{\perp}^2 \rangle$ is the square of the component of Ω_k perpendicular to the axis i averaged over the spin-oriented population and τ_p^* is the momentum scattering time of a *single* electron¹. Equation (1) reflects the diffusive character of the spin decoherence; the spin pseudovector performs a random walk on the surface of a sphere and its displacement from the initial position during a time t is proportional to $[\langle \Omega_{\perp}^2 \rangle \tau_p^* t]^{\frac{1}{2}}$ ($\tau_p^* \ll t \ll \tau_s$).

Equation (1) contains the ‘motional slowing’ characteristic of the DP mechanism; scattering actually inhibits spin reorientation so that increasing electron scattering produces slower spin relaxation. In the past it was assumed^{7,11,12} that τ_p^* could be equated to the momen-

tum relaxation time of the electron ensemble, τ_p , obtained from the electron mobility. In previous papers, Refs. 1,2,3,4, we have pointed out that this assumption is invalid in high-mobility *n*-type semiconductors. Furthermore, in 2DEGs, at low temperatures we have shown⁴ that the collision-dominated regime breaks down to give oscillatory¹³ rather than exponential spin evolution. Here we concentrate on spin dynamics of 2DEGs where the spin evolution is exponential and therefore the assumption of strong scattering is valid. We directly observe motional slowing and demonstrate that τ_p^* is, in general, much shorter than τ_p . Our theoretical analysis shows that this is a result of electron-electron scattering which can randomize spin precession whilst having almost no effect on the mobility. The conclusion is that, except at very low temperatures, electron-electron scattering is dominant in determining the spin dynamics in these 2DEGs. Furthermore it *increases* the relaxation time above that expected on the basis of scattering processes which limit the electron mobility.

II. EXPERIMENTAL TECHNIQUES AND RESULTS

The samples (see Table 1) used for our experiments were two series of one-side *n*-modulation doped single GaAs/AlGaAs quantum wells of widths L_z ranging from 6.8 nm to 20 nm and grown by MBE on (001)-oriented semi-insulating GaAs substrates. The first series designated T (for Toshiba) comprising nominal well widths of 20 nm and 10 nm consisted of the following layers: substrate, 1 micron GaAs, 1 micron AlGaAs, superlattice of 100 repeats of 2.5 nm GaAs and 2.5 nm AlGaAs, GaAs quantum well, 60 nm AlGaAs, 200 nm 10^{17} cm^{-3} Si-doped AlGaAs and 17 nm GaAs cap layer. The second series designated NU (Nottingham) with nominal well widths 10.2 nm and 6.8 nm had a different structure giving somewhat higher electron concentrations: substrate, 2 microns GaAs, 10.2 nm AlGaAs, seven repeats of 3.4 nm GaAs and 10.2 nm AlGaAs, GaAs quantum well, 30.4 nm AlGaAs, 30.4 nm 10^{18} cm^{-3} Si-doped AlGaAs and 25.4 nm GaAs cap layer. Except where specified all the layers were undoped and the Al fractional concentration was 0.33. They were fabricated into FET devices with transparent Schottky gate for optical measurements and Hall contacts to the conducting channel to allow control and *in situ* measurements of Hall mobility, μ , and electron concentration, N_S . The bias was set for maximum N_S which also corresponded to maximum μ in the wells. For low temperature measurements a liquid helium flow cryostat was used in which cold gas surrounded the sample.

Figure 1 shows Hall mobility measurements under the conditions of bias and illumination used for the optical investigation of spin-dynamics plotted as the corresponding ensemble momentum scattering time $\tau_p = \mu e/m_e$ where e is the elementary charge and m_e is the electron effective

mass. The values at the lowest temperatures are typical for high quality single quantum wells, as opposed to heterojunctions, with ensemble momentum relaxation times in the range 10 ps to 27 ps (see Table 1). These values are probably limited by neutral impurity and interface scattering. At higher temperatures the mobility falls off in a manner consistent with the onset of phonon scattering processes. The electron concentrations obtained from Hall measurements for each sample are constant up to at least 100 K and then fall off at higher temperatures. Above 100 K, however, the measurements become increasingly unreliable due to the possible existence of parallel conduction paths within the sample associated with thermally excited carriers. In our analysis (section III) we have used the measured values of mobility and assumed N_S to be temperature independent; as described below, we have used optical spectroscopy to determine the absolute value of N_S and hence Fermi temperature $T_F = E_F/k_B$, where E_F is the Fermi energy and k_B is the Boltzmann constant (Table 1).

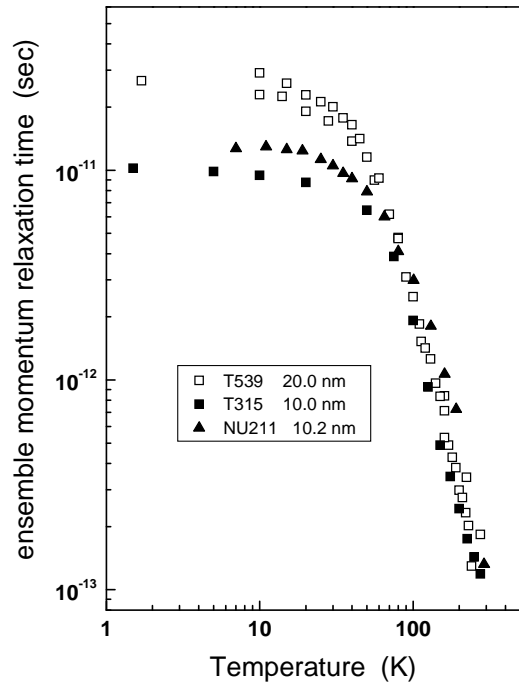


FIG. 1: Temperature dependence of the electron momentum relaxation time (from mobility) for different samples. The mobility in NU535 sample is essentially the same as in NU211 sample and is not shown here.

Figure 2 shows measurements of the photoluminescence (PL) and photoluminescence excitation (PLE) spectra of the samples at 5 K taken at the maximum value of N_S permitted by the sample design. In each case the PL peak corresponds to the transition between the conduction (CB) and valence (VB) band extrema (see inset) whereas the onset of PLE represents the interband transition to the lowest unoccupied conduction band states at the Fermi level. The energy difference

TABLE I: Sample parameters

	Nominal well width L_z (nm)	Electron confinement energy, E_{e1} (meV)	Electron density N_s (cm^{-3})	Fermi temperature T_F (K)	Ensemble momentum relaxation time τ_p (ps) at 5K	$\Omega(k_F)$ [5] (rad ps^{-1})	Single electron momentum relaxation time τ_p^* (ps) at 5K [5]
T539	20.0	10.2	$1.75 \cdot 10^{11}$	72	27	0.063 ± 0.006	22 ± 3
T315	10.0	49.8	$2.30 \cdot 10^{11}$	79	10	0.19 ± 0.01	6.0 ± 0.2
NU211	10.2	32.8	$3.10 \cdot 10^{11}$	129	13	0.22 ± 0.01	6.4 ± 0.9
NU535	6.8	58.5	$3.30 \cdot 10^{11}$	138	13	0.29 ± 0.02	5.1 ± 0.9

between the PL peak and the PLE onset was used to determine the electron concentration N_s using electron and hole effective masses of 0.067 and 0.13 respectively. These N_s values are more reliable than those obtained from the Hall measurements and we have used them in our analysis. The onset of the PLE shows a step or a peak characteristic of the Mahan exciton which has been studied previously in 2DEGs¹⁴. When biased for lower N_s the spectra showed features characteristic of negatively charged excitons¹⁵ rather than 2DEGs. Consequently we were not able to study effects of different concentrations in a true 2DEG in a single sample. Nevertheless the variation of concentration from sample to sample (Table 1) allows a direct test of theoretical predictions (see section III). Table 1 also contains measured values of the spin splitting at the Fermi surface $\Omega(k_F)$ and the electron momentum scattering time τ_p^* for each sample, obtained from the study of the spin dynamics of the samples in the quasi-collision-free low temperature regime⁵. This data is used in our theoretical analysis described in section III. The value of E_{e1} for each sample was calculated using PL and PLE spectra.

The spin-dynamics of the 2DEGs were investigated using a picosecond-resolution polarized pump-probe reflection technique¹⁶. Wavelength-degenerate circularly polarized pump and delayed linearly polarized probe pulses from a mode-locked Ti-sapphire laser were focused at close to normal incidence on the sample. Pump-induced changes of probe reflection ΔR and of probe polarisation rotation $\Delta\theta$ were recorded simultaneously as functions of probe pulse delay using balanced photodiode detectors and lock-in techniques. For ΔR , 10% beam splitters allowed comparison of intensities of the incident and reflected probe, and, for $\Delta\theta$, a polarising beam splitter gave comparison of reflected polarisation components at 45 degrees to the incident probe polarisation. The pump beam intensity was typically 0.5 mW focused to a 60 micron diameter spot giving an estimated photoexcited spin-polarized electron density $5 \times 10^9 \text{ cm}^{-2}$, very much less than the unpolarised electron concentration in the 2DEG (Table 1); probe power density was 25% of the pump.

At each temperature a wavelength excitation scan of

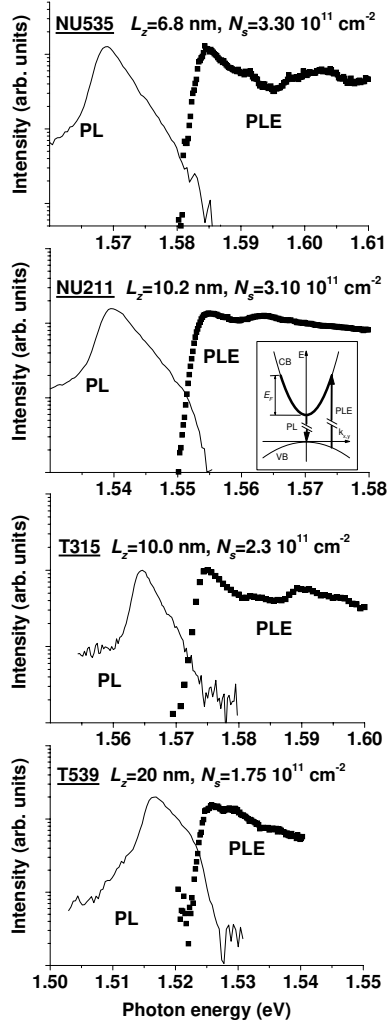


FIG. 2: Photoluminescence (PL) and photoluminescence excitation (PLE) spectra of the different samples at 5 K. The measurements were taken at the maximum value of N_s permitted by the sample design. The electron concentrations in the 2DEGs were determined from the energy difference between PL peak and PLE onset which involve interband transitions as indicated in the inset. Time-resolved pump-probe measurements of spin dynamics were carried out with the laser tuned to the PLE onset.

the ΔR and $\Delta\theta$ signals was recorded for a delay of 20 ps and measurements of the time evolution were then made at the wavelength of maximum signal. At low temperatures the maximum in $\Delta\theta$ coincided with the onset of the PLE spectrum in each sample (see Fig. 2).

On the time scale of this experiment, phase-space filling by the photoexcited electrons should dominate the pump-induced changes. The σ^+ circularly polarized pump photons will create an excess population of $|S_z = 1/2\rangle$ electrons at the Fermi energy with isotropic distribution of in-plane wave vectors and an equal population of $|J_z = -3/2\rangle$ holes in the valence band. The phase-space-filling effect of the holes may be neglected since they will rapidly relax into the lowest energy states available at the top of the heavy hole valence band, becoming depolarized at the same time. Furthermore, the majority of optical transitions from these states will already be blocked by the Fermi sea of electrons. The $\Delta\theta$ signal will therefore be proportional to the pump-induced imbalance of electron spin polarization along the growth axis z , $\langle S_z \rangle$, and ΔR to the density of photoexcited electrons.

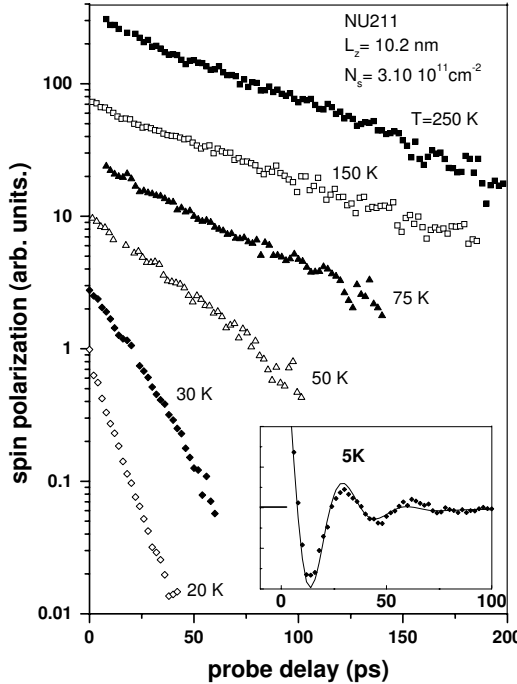


FIG. 3: Time evolution of the $\Delta\theta$ signal and hence the spin polarization for NU211 sample for a range of temperatures. At 20 K and above the evolution is exponential with rapidly increasing decay time. At 5 K, oscillatory behaviour was observed (inset) and was analysed by Monte-Carlo techniques (solid)⁵ to give directly $\Omega(k_F)$ and τ_p^* .

Figure 3 shows the time evolution of $\Delta\theta$ for sample NU211 at several different temperatures; the traces are offset vertically from one another for clarity. ΔR was essentially constant for this range of delays indicating negligible decay of the photoexcited population. Thus

the behaviour of $\Delta\theta$ indicates the pure spin-relaxation of the electrons. It can be seen that the decay time increases very rapidly as the temperature is raised, consistent with decrease of τ_p^* in Eq. (1) (the value of $\langle \Omega_\perp^2 \rangle$ should not be strongly temperature dependent, see section III). The inset shows the behaviour of $\Delta\theta$ at 5 K; the spin evolution is oscillatory rather than exponential and analysis using a Monte Carlo simulation technique^{4,5} gives the frequency $\Omega(k_F)$ and the scattering time τ_p^* (Table 1).

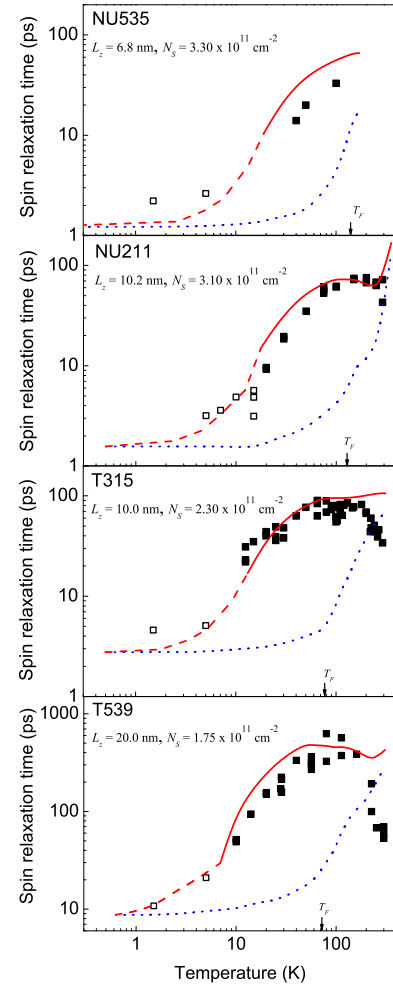


FIG. 4: Spin relaxation times vs. temperature. The points present the experimental results; solid squares are directly measured exponential decay times whereas open squares are values of $[\Omega(k_F)^2 \tau_p^*]^{-1}$ for cases of oscillatory spin evolution. Lines are the theoretical results calculated using the experimental values of the ensemble momentum relaxation times including (solid) and not including (dotted) electron-electron collisions.

Figure 4 shows the values of τ_s measured as a function of temperature in the four samples. The solid symbols are from direct measurements of exponential decay. The

open symbols, at low temperatures, do not represent exponential decay but are values of $[\Omega(k_F)^2 \tau_p^*]^{-1}$ obtained from the observed oscillatory spin evolution⁵. For each of the samples τ_s increases rapidly with temperature and for the three larger values of L_z passes through a maximum at a temperature which corresponds approximately to the Fermi temperature, indicated by the arrows. For sample NU535 the same trend is observed but there are insufficient points to identify a maximum in the variation. There is also a clear trend towards lower τ_s for smaller well width. The curves in Fig. 4 are the result of our theoretical calculations described in section III; the solid and dashed curves represent calculated spin relaxation times based on the DP mechanism and including both electron-electron and ensemble momentum scattering whereas the dotted curves are the same calculations but including only the ensemble momentum scattering obtained from the measured mobility.

III. DISCUSSION

A. Quantitative calculations

Here we give an outline of the quantitative theory which we use to interpret the experimental results; full details have already been published in Refs. [3] and [19]. We use the kinetic theory and describe spin-polarized electrons in the framework of the spin-density matrix $\rho_{\mathbf{k}} = f_{\mathbf{k}} + \sigma \mathbf{s}_{\mathbf{k}}$, where $f_{\mathbf{k}}$ is the electron distribution function and $\mathbf{s}_{\mathbf{k}}$ is the average spin of an electron in the state with wave vector \mathbf{k} . Since the optical excitation evidently makes no essential changes in the distribution function $f_{\mathbf{k}}$, it is enough to consider the time evolution of the spin distribution function $\mathbf{s}_{\mathbf{k}}$ only. The spin distribution function satisfies the pseudovector kinetic equation which, with allowance for electron-electron interaction, reads³

$$\frac{d\mathbf{s}_{\mathbf{k}}}{dt} + \mathbf{s}_{\mathbf{k}} \times (\boldsymbol{\Omega}_{\mathbf{k}} + \boldsymbol{\Omega}_{C,\mathbf{k}}) + \mathbf{Q}_{\mathbf{k}}\{\mathbf{s}\} = 0, \quad (2)$$

where $\mathbf{Q}_{\mathbf{k}}\{\mathbf{s}\}$ is the collision integral, $\boldsymbol{\Omega}_{\mathbf{k}}$ and $\boldsymbol{\Omega}_{C,\mathbf{k}}$ are the effective spin precession frequencies due respectively to the spin-splitting and to the electron-electron exchange interaction.

In a quantum well there are three potential contributions to the spin-splitting $\boldsymbol{\Omega}_{\mathbf{k}}$ (Refs. [7,17]) originating from inversion asymmetry of the crystal structure (Dresselhaus or BIA), from asymmetry of the quantum well structure and applied odd parity perturbations such as electric field (Rashba or SIA) and from asymmetry of atomic arrangement at interfaces (NIA). The NIA term may be ignored for GaAs/AlGaAs structures⁷. The BIA and SIA contributions each have a leading term linear in \mathbf{k} giving total e1 subband splitting

$$\frac{\hbar}{2} (\boldsymbol{\sigma} \cdot \boldsymbol{\Omega}_{\mathbf{k}}) = \beta_1 (\sigma_y k_y - \sigma_x k_x) + \beta_2 (\sigma_x k_y - \sigma_y k_x), \quad (3)$$

where β_1, β_2 are the constants describing BIA and SIA contributions respectively and x and y are the crystallographic axes [100] and [010]. The distinctive feature of the BIA term is the factor $\langle k_z^2 \rangle$ in β_1 , where k_z is the wavevector component along the growth axis¹². We note that it arises as a quantum mechanical average of the cubic-in- \mathbf{k} splitting in bulk zinc-blende semiconductors and $\langle k_z^2 \rangle$ is proportional to the electron confinement energy, E_{e1} .

The electron-electron exchange splitting is given by

$$\boldsymbol{\Omega}_{C,\mathbf{k}} = \frac{2}{\hbar} \sum_{\mathbf{k}'} V_{\mathbf{k}'-\mathbf{k}} \mathbf{s}_{\mathbf{k}'}, \quad (4)$$

where $V_{\mathbf{q}}$ is the Fourier transform of the screened 2D Coulomb potential. The full expression for the electron-electron scattering contribution to the collision integral is given in Refs. [3,19] (see also Ref. [20]) and is not presented here. The momentum relaxation processes governing the electron mobility are described in the framework of the temperature-dependent scattering time $\tau_p(T)$.

For the samples under study the electron polarisation P_s is of order of 1% and the $\boldsymbol{\Omega}_{C,\mathbf{k}}$ (Hartree-Fock) term in Eq. (2) can be ignored³.

Assuming $\Omega_{\mathbf{k}} \tau_p^* \ll 1$, which is valid for the temperatures exceeding 10 K to 20 K depending on the sample, Eq. (2) can be solved by iteration in this small parameter leading to exponential decay of the total electron spin: $\mathbf{S}(t) = \mathbf{S}_0 \exp(-t/\tau_s) \parallel z$. While solving Eq. (2) the spin distribution function $\mathbf{s}_{\mathbf{k}}$ is represented as a sum $\mathbf{s}_{\mathbf{k}}^0 + \delta \mathbf{s}_{\mathbf{k}}$ where $\mathbf{s}_{\mathbf{k}}^0$ is the quasi-equilibrium function, and the correction $\delta \mathbf{s}_{\mathbf{k}} \propto \Omega_{\mathbf{k}} \tau_p^*$ arises due to the spin precession. This correction is determined from the linearized equation with the result³

$$\delta \mathbf{s}_{\mathbf{k}} = F_{\mathbf{k}} \mathbf{S}(t) \times \boldsymbol{\Omega}_{\mathbf{k}}, \quad (5)$$

where $F_{\mathbf{k}}$ is a function independent of the wave-vector direction. Finally, one can arrive to the following expression for the zz component of the tensor of spin relaxation rates

$$\frac{1}{\tau_s} = \sum_{\mathbf{k}} |\boldsymbol{\Omega}_{\mathbf{k}}|^2 F_{\mathbf{k}} = \frac{4}{\hbar^2} (\beta_1^2 + \beta_2^2) \sum_{\mathbf{k}} k^2 F_{\mathbf{k}}. \quad (6)$$

In Fig. 4 we show theoretical curves for τ_s calculated using Eq. (6); the solid and dashed curves were calculated taking into account both electron-electron collisions and the ensemble scattering processes using the measurements of $\tau_p(T)$ (Fig. 1); the dotted curves were calculated including only the ensemble scattering. In the high temperature regime (solid portion of curve) where $\Omega_{\mathbf{k}} \tau_p^* \lesssim 1$ the theory predicts exponential spin relaxation and values of τ_s can be compared directly with the experimental decay times (solid symbols). In the low temperature regime where $\Omega_{\mathbf{k}} \tau_p^* \gtrsim 1$ the spin dynamics become oscillatory and quantities calculated using Eq. (6) (dashed portion of curve) do not represent exponential decay times. They can however be directly compared with the values

of $[\Omega(k_F)^2 \tau_p^*]^{-1}$ (open symbols) obtained from the observed oscillatory spin evolution.

The calculations have no adjustable parameters. The parameters used are all determined independently and are given in Table 1; they are well width (L_z), barrier height (determined by Al concentration), scattering time $\tau_p(T)$ (from mobility), electron concentration (N_S) and the spin splitting constant $\sqrt{\beta_1^2 + \beta_2^2}$ [obtained from the measured values of $\Omega(k_F)$]. From the PL peak positions in Fig. 2 it is clear that the true well widths, particularly for NU211 and T315 are somewhat different than the nominal ones. The well-width enters directly only in the calculation of the electron-electron scattering; although we used the nominal values of well width the errors involved will be small because the electron-electron scattering times are not strongly dependent on well width². The well width also has a stronger indirect effect via the value of $\Omega(k_F)$ which is measured for each sample.

B. Qualitative interpretation of the spin relaxation

Before considering in detail the comparison of the calculations with experiment we give qualitative arguments which provide a physical understanding of the temperature, concentration and well-width dependence of the spin relaxation time shown in Fig. 4. Returning to Eq. (1), we see that the spin relaxation time is inversely proportional to the product of the average squared spin precession frequency and the scattering rate.

Let us first consider $\langle \Omega_\perp^2 \rangle$. Both SIA and BIA terms are linear in the in-plane wavevector. This means that at relatively low temperatures where electron confinement energy exceeds the thermal energy, to a first approximation Ω_k is linear in the in-plane electron wavevector and $\langle \Omega_\perp^2 \rangle$ is proportional to the average in-plane kinetic energy. For a degenerate electron gas the latter is independent of T and proportional to Fermi temperature $T_F \sim N_S$ (we remind that $T_F = E_F/k_B$). For BIA spin splitting at temperatures less than E_{e1}/k_B , $\langle \Omega_\perp^2 \rangle$ should be approximately proportional to $E_{e1}^2 E_F$. This tendency is consistent with the data given in Table 1, see also Ref. 5. For a non-degenerate 2DEG $\langle \Omega_\perp^2 \rangle$ is linear in T and independent of N_S . Note, that in the temperature range of our experiments $\langle \Omega_\perp^2 \rangle$ changes by no more than a factor of 3.

Now consider the scattering rate $(\tau_p^*)^{-1}$. If we ignore electron-electron scattering, $(\tau_p^*)^{-1}$ will follow the inverse of the mobility (see Fig. 1), constant at low temperatures and increasing roughly as T^2 at high temperatures where phonon scattering takes over. Combining this with the variation of $\langle \Omega_\perp^2 \rangle^{-1}$ gives a contribution to the temperature dependence of τ_s which is constant at low temperature and roughly proportional to T at high temperatures. This is indicated by the dashed curve in Fig. 5, which follows qualitatively the dotted curves in Fig. 4.

Our next step is to include the electron-electron scattering. Physically, the collisions between electrons

change randomly the orientation of the wavevector of a given electron and, if the spins of colliding electrons are different, leads to randomization of the precession frequencies Ω_k exactly as for other scattering processes. For a degenerate electron gas the electron-electron scattering rate of an electron near the Fermi energy is governed by the Pauli-exclusion principle. Phase-space arguments¹⁸ demonstrate that for a pair of electrons the number of free final states is proportional to the squared ratio of temperature and Fermi energy. According to Ref. [3] the effective scattering rate which is relevant to the D'yakonov-Perel' spin relaxation mechanism has, for a strictly 2D system, the form

$$\frac{1}{\tau_{ee}} \approx 3.4 \frac{E_F}{\hbar} \left(\frac{k_B T}{E_F} \right)^2, \quad T \ll T_F. \quad (7)$$

The Fermi level E_F is proportional N_S giving

$$\tau_{ee}^{-1} \sim T^2 N_S^{-1} \quad T \ll T_F. \quad (8)$$

This counter-intuitive concentration dependence arises because, for a fully degenerate electron gas, i.e. at $T=0$ K, the electron-electron scattering rate vanishes due to Pauli exclusion principle. At a finite temperature the rate becomes finite but now any change which moves the system back towards full degeneracy, such as increase of electron concentration, will produce a reduction in the scattering rate. For a nondegenerate electron gas the electron-electron scattering rate is determined by the wavevector dependence of the Coulomb matrix element and the density of electrons. Thus³,

$$\tau_{ee}^{-1} \approx 35.7 \frac{e^4 N_S}{\hbar a^2 k_B T} \sim N_S T^{-1}, \quad T \gg T_F. \quad (9)$$

Combining expressions (8) and (9) with $\langle \Omega_\perp^2 \rangle^{-1}$ gives

$$\tau_s \sim \begin{cases} T^2 N_S^{-2}, & T \ll T_F, \\ T^{-2} N_S, & T \gg T_F. \end{cases} \quad (10)$$

These contributions for one value of N_S are shown as the dotted curve in Fig. 5 (the region near $T = T_F$ being no more than a guide to the eye) and the combined effect of the different scattering processes is given by the solid curve.

Clearly these considerations give no more than a very crude qualitative picture but nonetheless contain the essential physical explanation of the observed rapid increase with temperature of the spin relaxation time as well as the observed maxima for the different samples. On the assumption that the BIA term is dominant we expect that $\langle \Omega_\perp^2 \rangle \sim E_{e1}^2$ and therefore, other factors remaining constant, that the spin relaxation time at a given temperature will scale as E_{e1}^{-2} or approximately as L_z^4 . This is a somewhat stronger dependence than we observe experimentally as can be seen from Fig. 4. The actual behaviour must be understood by inclusion also of the differences of τ_p^* and in the relative importance of the SIA and BIA terms for different samples.

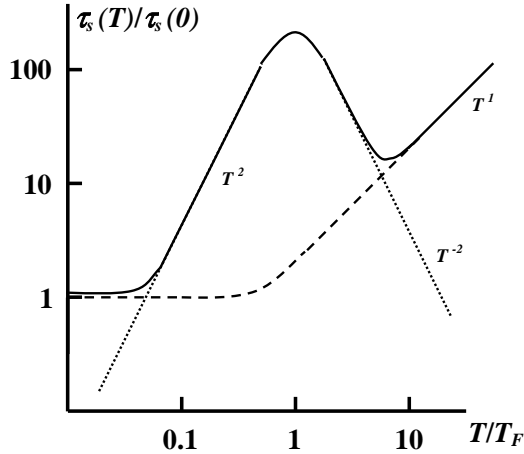


FIG. 5: Qualitative picture of the temperature dependence of the spin relaxation time. Dashed curve presents the contribution of the ensemble momentum scattering processes. Dotted curve is the prediction for electron-electron collisions only. The solid curve is the combined total spin relaxation time.

C. Comparison of quantitative calculations with experiment

It is clear from Fig. 4 and the arguments leading to Fig. 5 that a proper description of the temperature dependence of the spin relaxation requires inclusion of electron-electron scattering; calculation neglecting electron-electron collisions does not fit the experimental points but agreement when including electron-electron scattering is excellent. In particular the calculation reproduces very well the observed rapid increase of spin relaxation time with temperature between 10K and 100K and also the observed maxima which occur close to the transition temperature T_F between degenerate and non-degenerate regimes of the 2DEG.

The only significant disagreement between theory and experiment is above about 200 K in samples T315 and T539; here the trend of the theory is upwards with temperature due to the fact that, in this range, the ensemble momentum scattering rate is dominating over the electron-electron scattering; at the same time the experimental points are falling with temperature. This could indicate the presence in the samples of some spin-relaxation process other than the DP mechanism or, if the explanation stays within the DP mechanism (Eq (1)) either that total electron momentum scattering is weaker than we have assumed or that the precession term $\langle \Omega_{\perp}^2 \rangle$ is stronger. Below we briefly discuss these possible reasons for the discrepancy.

First, we exclude spin relaxation mechanisms other than DP. The Bir-Aronov-Pikus (BAP) mechanism^{6,7,10} is irrelevant as electrons are the major carriers in the samples under study. We believe also that paramagnetic impurities²¹ play no role as there is no evidence of their presence and furthermore such a scattering cannot result

in strong temperature dependence of the spin relaxation time as we observe here. The Elliott-Yafet (EY) mechanism^{6,7,8,9,22,23}, where the spin relaxation occurs due to spin-flip scattering is unimportant at high temperatures even in bulk GaAs and is further suppressed in quantum wells. For an estimate of the spin relaxation time one may use $\tau_s(T) \sim 10^5 \tau_p(T)$ (see Ref. [24]), which gives, for our lowest value of $\tau_p \sim 10^{-13}$ s (Fig. 1), $\tau_s \sim 10^{-8}$ s, at least two orders of magnitude larger than the experimental values.

Thus, we come to the conclusion that the spin relaxation in the temperature range 200 K to 300 K is governed by the DP mechanism. One way in which we could have underestimated $\langle \Omega_{\perp}^2 \rangle$ is if our assumption of temperature-independence of $\beta_1^2 + \beta_2^2$ in Eq. (6) were to break down. In principle this could occur if, in the high-temperature regime, built-in electric fields vary in the sample causing the coefficient of the SIA term β_2 to play an increasing role. However, estimates of the electric field required to explain the effect (~ 100 kVcm⁻¹) make this unlikely.

Finally we examine the possibility that the discrepancy can be explained by an overestimation of the electron scattering rate used in the calculations. In the worst case, T539 at 300 K (Fig. 4), we see that not only is a tenfold reduction in the overall scattering rate required but also, since the dotted curve lies above the experimental points, a reduction of the ensemble scattering rate by at least a factor 3 is required, implying that our Hall measurements have underestimated the mobility by that factor at 300 K. The remaining discrepancy would then disappear if the well were completely depleted of electrons by 300 K rather than the electron concentration being constant, as we assume in calculating the solid curves. We cannot rule out such an error in the mobility since we are unable to assess the effects of transport in other parts of the sample than the 2DEG and, furthermore, as mentioned in section II, the Hall measurements do indicate some reduction of concentration at higher temperatures. Therefore it is most likely that the discrepancies at high temperature in Fig. 4 are due to errors in the mobility and concentration measurements and do not imply a fundamental lack of physical understanding of the system.

IV. CONCLUSION

We have made a comprehensive experimental and theoretical study of the electron spin relaxation in 2DEGs in quantum wells with different widths, carrier concentrations and carrier mobilities. The main observations are of rapid increase of the spin-relaxation time between 10 K and 100 K to a maximum at a temperature close to the Fermi temperature of the 2DEG. The main spin relaxation mechanism, namely, the Dyakonov-Perel' mechanism is identified for all the samples in the whole temperature range under study. We have made Hall measurements of electron mobility to determine the momentum

scattering rate for the electron ensemble and measurements of the low temperature spin beats⁵ allowed us to directly determine the spin precession rate at the Fermi level. It turns out that the elastic momentum scattering processes which govern the electron mobility *do not* play an important role in the spin relaxation for the temperature range 10 K – 150 K. The only possible candidate is thus *electron-electron collisions* which conserve the total momentum of the pair but contribute to the randomization of the spin precession frequencies. The experimental results and our theoretical calculations (made without fitting parameters) are in good agreement with each other. We conclude that the spin dynamics in high-mobility

n-type quantum wells is determined by the Dyakonov-Perel' (or precessional) spin relaxation mechanism, governed by electron-electron collisions.

Acknowledgments

The work was supported financially by RFBR, “Dynasty” foundation – ICFPM, the Engineering and Physical Sciences Research Council (EPSRC) and the Royal Society.

-
- ^{*} Permanent address: Cavendish Laboratory, Madingley Road, Cambridge CB4 3HE, UK.
- ¹ M.M. Glazov and E.L. Ivchenko, JETP Lett. **75**, 403 (2002).
- ² M.M. Glazov, Phys. Sol. State **45**, 1162 (2003).
- ³ M.M. Glazov and E.L. Ivchenko, JETP **99**, 1279 (2004).
- ⁴ M.A. Brand, A. Malinowski, O.Z. Karimov, P.A. Marsden, R.T. Harley, A.J. Shields, D. Sanvitto, D.A. Ritchie, and M.Y. Simmons, Phys. Rev. Lett. **89**, 236601 (2002); M.M. Glazov, W.J.H. Leyland, E.L. Ivchenko, R.T. Harley, M. Henini, A.J. Shields, and D.A. Ritchie, Proceedings of 28th International Conference on Physics of Semiconductors (ICPS 28) Vienna, 2006; M.M. Glazov, E.L. Ivchenko, M.A. Brand, O.Z. Karimov, and R.T. Harley, Proc. Int. Symp. “Nanostructures: Physics and Technology” (St. Petersburg, Russia, 2003).
- ⁵ W.J.H. Leyland, R.T. Harley, M. Henini, A.J. Shields, and D.A. Ritchie, Proceedings of 28th International Conference on Physics of Semiconductors (ICPS 28) Vienna, 2006, and to be published.
- ⁶ F. Meier and B.P. Zakharchenya (ed.) 1984 *Optical Orientation, Modern Problems in Condensed Matter Science* (Amsterdam: North-Holland)
- ⁷ M.E. Flatté, J.M. Byers, and W.H. Lau 2002 *Semiconductor Spintronics and Quantum Computation: chapter 4, Spin Dynamics in Semiconductors*, ed. D.D. Awschalom *et al.* (Berlin: Springer)
- ⁸ R.J. Elliott, Phys. Rev. **96**, 266 (1954).
- ⁹ Y. Yafet 1963 in *Solid State Physics*, Vol. 14, ed. F. Seitz and D. Turnbull (Academic, New York), p. 2.
- ¹⁰ G.L. Bir, A.G. Aronov, and G.E. Pikus, Sov. Phys. JETP **42**, 705 (1976).
- ¹¹ M.I. D'yakonov and V.I. Perel', Sov. Phys. JETP **33**, 1053 (1971); Sov. Phys. Solid State **13**, 3023 (1971).
- ¹² M.I. D'yakonov and V.Yu. Kachorovskii, Sov. Phys. Semicond. **20**, 110 (1986).
- ¹³ V.N. Gridnev, JETP Lett. **74**, 380 (2001)
- ¹⁴ S.R. Andrews, R.T. Harley, A.S. Plaut, and T.M. Kerr, Phys. Rev B **41**, 5040 (1990).
- ¹⁵ R. Kaur, A.J. Shields, J.L. Osborne, M.Y. Simmons, D.A. Ritchie, and M. Pepper, Phys. Stat. Sol. (a) **178**, 465 (2000).
- ¹⁶ R.T. Harley, O.Z. Karimov, and M. Henini, J. Phys. D: Appl. Phys. **36**, 2198 (2003).
- ¹⁷ E.L. Ivchenko and G.E. Pikus, *Superlattices and Other Heterostructures: Symmetry and Optical Phenomena*, Springer Series in Solid State Sciences, vol. 110, Springer-Verlag, 1995; 2nd edition 1997.
- ¹⁸ G.F. Giuliani and J.J. Quinn, Phys. Rev. B **26**, 4421 (1982); L. Zheng and S. Das Sarma, Phys. Rev. B **53**, 9964 (1996).
- ¹⁹ M.M. Glazov and E.L. Ivchenko 2003 in *Optical Properties of 2D Systems with Interacting Electrons* ed. W.J. Ossau and R. Suris, p. 181.
- ²⁰ M.Q. Weng, M.W. Wu, and L. Jiang, Phys. Rev. B **69**, 245320, (2004).
- ²¹ I. Zutic, J. Fabian, and S. Das Sarma, Rev. Mod. Phys **76**, 323 (2004).
- ²² Z.G. Yu, S. Krishnamurthy, M van Schilfgaarde, and N. Newman, Phys. Rev. B **71**, 245312 (2005).
- ²³ Pil Hun Song and K.W. Kim, Phys. Rev. B **66**, 035207 (2002).
- ²⁴ N.S. Averkiev, L.E. Golub, and M. Willander, J. Phys.: Condens. Matter **14**, R271 (2002).